

Non-linear effect of uniaxial pressure on superconductivity in CeCoIn₅

S. D. Johnson and R. J. Zieve

Physics Department, University of California Davis, Davis, CA 95616

J. C. Cooley

Los Alamos National Laboratory, Los Alamos, NM 87545

(Dated: December 6, 2019)

We study single-crystal CeCoIn₅ with uniaxial pressure up to 3.97 kbar applied along the *c*-axis. We find a non-linear dependence of the superconducting transition temperature T_c on pressure, with a maximum close to 2 kbar. The transition also broadens significantly as pressure increases. We discuss the temperature dependence in terms of the general trend that T_c decreases in anisotropic heavy-fermion compounds as they move towards three-dimensional behavior.

I. INTRODUCTION

The past three decades have seen the discovery of several new groups of superconductors that do not conform to the previous understanding of superconductivity: the cuprates [1], heavy fermions [2], organics [3], and the very recent pnictide superconductors [4]. Although behavior varies substantially among these materials, in many cases even for closely related compounds, similarities include deviations from Fermi liquid behavior [5–8] and the appearance of superconductivity near the quantum critical point where a magnetic transition is suppressed to zero temperature [9–11]. From these observations a general picture is emerging of superconductivity with Cooper pairs bound by magnetic fluctuations. The magnetic interaction favors the *d*-wave pairing symmetry which has been established in the cuprates [12] and indicated elsewhere [13–16]. Low dimensionality also facilitates superconductivity [17, 18], since the pairing interaction falls off less quickly in lower dimensions.

The 115 superconductors, CeMIn₅ ($M = \text{Co}$ [19], Rh [20], Ir [21]) and the isostructural PuMGa₅ ($M = \text{Co}$ [22], Rh [23]) family, are useful materials for testing effects of dimensionality. Both families are heavy-fermion superconductors that also exhibit antiferromagnetism, sometimes in concert with superconductivity. They are clean, relatively easy to grow, and close to a quantum critical point at ambient pressure. The crystal structure is tetragonal, with alternating layers of CeIn₃ and MIn₂, resulting in anisotropic superconductivity. For the 115 materials, including several alloys where *M* is a mixture of two elements, the superconducting transition temperature T_c increases linearly with *c/a* within a family [24], with the same logarithmic derivative $\frac{d(\ln T_c)}{d(c/a)}$ for both the Ce and Pu families [25]. In several cases uniaxial pressure adheres to this trend. By pushing the planes together, *c*-axis pressure should decrease T_c . On the other hand, *a*-axis pressure increases the plane separation and should increase T_c . For CeIrIn₅, uniaxial pressure has exactly these effects, with measurements made both directly [26] and by extracting the zero-pressure dT_c/dP from thermal expansion data [27]. However, for CeCoIn₅ thermal expansion measurements yield positive $\frac{dT_c}{dP}|_{P=0}$ for *c*-axis

pressure as well as *a*-axis pressure [27]. Here we apply uniaxial pressure along the *c*-axis of CeCoIn₅ to investigate this apparent exception to the pattern that higher dimensionality corresponds to lower T_c .

II. MATERIALS & METHODS

Single crystal samples were grown in aluminum crucibles containing stoichiometric amounts of Ce and Co with an excess of In. The crucibles were sealed in quartz tubes, heated to 1150° C, and slow cooled to 450° C. Excess flux was removed by centrifuging. CeCoIn₅ grows in thin platelets perpendicular to the crystal *c*-axis. To prepare samples for pressure measurements, we remove excess In and polish the faces to be smooth and free from chips or defects. The polishing also ensures that the faces used for pressure application are parallel to each other. We confirm the sample orientation by x-ray diffraction, both before and after polishing.

We apply uniaxial pressure using a bellows setup activated with helium gas from room temperature. The pressure cell is permanently mounted on an Oxford dilution refrigerator. A piezo sensor monitors the force in the pressure column (see [26] for pressure setup schematic). With this setup we can reach a maximum pressure of about 10 kbar, depending on the cross-sectional area of the sample, and we can change pressure in controlled steps smaller than 0.1 kbar.

From the mass and thickness of the sample, we compute its cross-sectional area, which we then use to calculate the pressure on the sample. The data shown here are from a sample with mass 2.43 mg and area $1.54 \times 10^{-6} \text{ m}^2$. Measurements of a second sample of mass 0.57 mg and area $3.63 \times 10^{-7} \text{ m}^2$ agreed qualitatively, although the smaller sample size reduced the quality of the data.

A screw at one end of the pressure column controls its overall length. We finger-tighten this screw while watching the pressure monitor, applying a pressure of about 0.05 kbar to the sample at room temperature. This ensures that the sample remains in place while we load the cryostat into its dewar and cool from room temperature. Thermal contraction during cooling may alter the

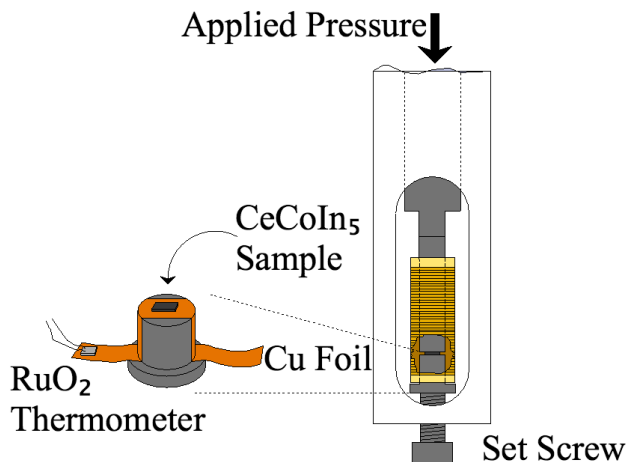


FIG. 1: A balanced ac-susceptibility coil is placed around the pressure shafts. The sample is between the two shafts of the pressure column, centered in one of the pick-up coils.

initial pressure; in previous work the initial pressure appeared on the order of 0.3 kbar at low temperatures [26]. The values for applied pressure used in this paper do not include any offset for this initial pressure, but our initial transition temperature measurements agree to better than 3 mK with measurements taken outside of the pressure cell, suggesting a pressure offset of less than 0.2 kbar. Once the cryostat is below 4 K we fill the bellows with liquid helium. We then increase pressure in steps of about 0.5 kbar. The maximum pressure used here is 3.97 kbar.

We detect the transition to the superconducting state with a balanced ac susceptibility coil that accommodates the pressure shafts and the sample, as shown in Figure 1. The outer primary coil is 0.9 inches long with inner diameter 0.35 inches. It contains approximately 600 turns of 0.006-inch diameter Cu wire and with our usual settings generates a field of about 0.3 gauss parallel to the pressure shafts. The inner secondary coils are wound on a former of diameter of 0.16 inches and contain 200 turns each of 0.002-inch diameter Cu wire. The inner coils are separated by 0.325 inches, so that there is minimal field interaction between coils. We monitor the signal from the inner coils using a Linear Research LR-700 resistance bridge. We position the sample so that its entire volume is contained within the bottom coil of the secondary.

To ensure that the sample is in thermal contact with the mixing chamber we varnish Cu foil to the pressure shafts on either side of the sample, with the other end of each foil varnished to the mixing chamber. Even with the Cu foil heat-sink, the large thermal mass of the pressure setup results in a temperature lag between the sample and the mixing chamber during temperature scans. We monitor the sample temperature directly using a RuO₂ thermometer mounted on the copper foil within 0.5 inches of the sample.

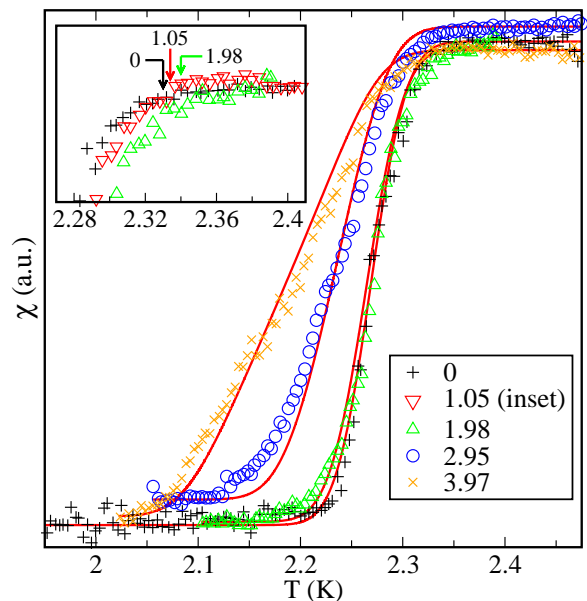


FIG. 2: Representative data showing the effect of c -axis uniaxial pressure. The transition width ΔT_c is strongly pressure-dependent, while the onset temperature T_c is not. The inset expands the region near T_c to reveal a slight increase in T_c with pressure. Arrows indicate the onset T_c for each curve.

III. RESULTS

Figure 2 shows the superconducting transition for four different pressures. The substantial broadening of the transition with pressure ensures that the midpoint moves down in temperature with increasing pressure. However, as shown in the inset, the onset behaves differently, initially moving to *higher* temperature as pressure increases. Here we identify the onset as the highest temperature at which the susceptibility χ deviates from its constant normal-state value χ_n . We plot the onset temperatures T_c in Figure 3. The dashed parabola, with a maximum near 2 kbar, is a least-squares fit.

The non-monotonic $T_c(P)$ makes it particularly important to consider the meaning of the transition width. The width ΔT_c , defined as the difference between onset of superconductivity and the leveling off of χ at the low end of the transition, increases from 112 mK at zero pressure to 270 mK at 3.97 kbar. One possible source for the broadening is non-uniformity in the applied pressure. The pressure dependence of T_c would then lead to different transition temperatures in different parts of the sample. Non-uniform pressure could arise from a variety of effects, such as defects in the sample, variation in its cross-sectional area, indium inclusions, surface irregularities, a tilt in the pressure column, or an intrinsic inhomogeneity in the pressure distribution within the sample.

We introduce a model to explore how the non-linear pressure dependence could combine with non-uniform

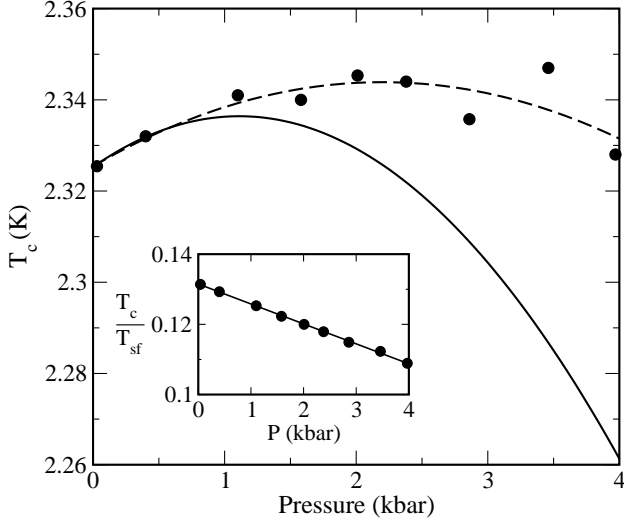


FIG. 3: Onset temperature for superconductivity as a function of pressure. Solid circles: averages over measurements at similar applied pressures P_{app} . Dashed line: quadratic fit to onset data. Solid line: transition onsets if all broadening is due to pressure inhomogeneity (see text). Inset: T_c/T_{sf} vs. pressure, with a linear fit shown. As described in the text, T_{sf} values are adapted from hydrostatic pressure measurements.

pressure to produce the observed susceptibility. We first define a function $f(P/P_{app})$, representing the fraction of the sample that feels an actual pressure P when the applied pressure is P_{app} . Using relative pressure $p \equiv P/P_{app}$ as the argument of f ensures that the pressure distribution scales with pressure. This would be a natural assumption if the pressure variations arise from the sample's not having a constant cross-sectional area or from a slight angle in the pressure column. It is supported by the linear increase of ΔT_c with pressure, shown in Figure 4.

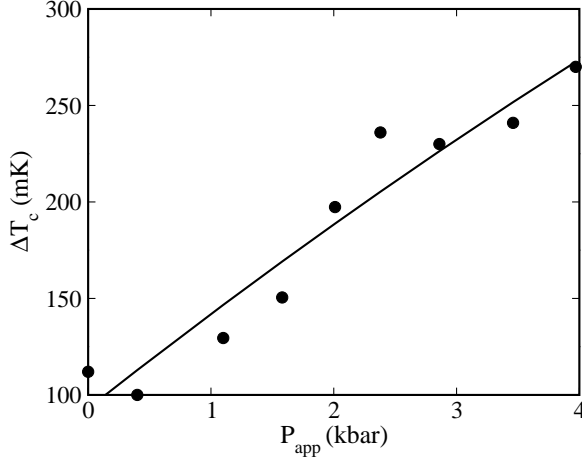


FIG. 4: Superconducting transition width versus applied pressure. Solid line is the best linear fit to the data.

Each portion of the sample is at some pressure. This gives a normalization requirement for the pressure distribution function:

$$1 = \int_0^\infty f(p) dp. \quad (1)$$

Also, since the total force on the sample is determined by the known force in the pressure column, the average pressure on the sample equals the nominal applied pressure, P_{app} . Equivalently the average relative pressure is 1:

$$1 = \int_0^\infty p f(p) dp. \quad (2)$$

We next describe the finite width of the transition in the absence of applied pressure. We treat the sample as being slightly inhomogeneous, with a Gaussian distribution of transition temperatures. The distribution is centered at T_c with width σ . At temperature T , a fraction F of the sample has $T_c < T$ and is in the normal state; the remainder is superconducting. We find F by integrating over the distribution, $F = \frac{1}{\sigma\sqrt{\pi}} \int_0^T e^{-\frac{(T' - T_c)^2}{\sigma^2}} dT'$. At very low temperature F goes to zero, while at high temperature F approaches one. The corresponding susceptibility is

$$\chi(T) = \chi_n F + \chi_{sc}(1 - F). \quad (3)$$

Note that here T_c is the midpoint of the transition. We determine the intrinsic transition width σ and zero-pressure transition temperature by fitting the zero-pressure data to Equation 3.

We assume, for now, that the only effect of perfectly uniform pressure is to shift the Gaussian so that it is centered at $T_c(P)$, without changing its width. For non-uniform pressure, the pressure-dependent shift in T_c varies across the sample, which can broaden the observed transition. Overall, the susceptibility obeys

$$\chi(T, P_{app}) = \int_0^\infty f(p) \left[\chi_{sc} + \frac{\chi_n - \chi_{sc}}{\sigma\sqrt{\pi}} \int_0^T e^{-\frac{(T' - T_c(pP_{app}))^2}{\sigma^2}} dT' \right] dp$$

where $T_c(P)$ gives the true pressure dependence of the superconducting transition temperature. Motivated by the observed pressure dependence of the onset temperature, we take $T_c(P) = T_c(0) + A_1 P + A_2 P^2$.

We use two forms for the pressure distribution function $f(p)$. The first is a quadratic function defined by $f(p) = f_0 + f_1 p + f_2 p^2$ for $0 < p < p_{max}$ and vanishing outside this range. This expression contains four coefficients (f_0, f_1, f_2, p_{max}). Equations 1 and 2 provide two constraints on these coefficients, which

we use to write $f_0 = \frac{1}{6}f_2p_{max}^2 + \frac{4}{p_{max}} - \frac{6}{p_{max}^2}$ and $f_1 = -f_2p_{max} - \frac{6}{p_{max}^2} + \frac{12}{p_{max}^3}$. We then fit $\chi(T, P_{app})$ to susceptibility data at all pressures, finding the simultaneous best fit with respect to the free parameters f_2 , p_{max} , A_1 , and A_2 . The resulting $f(p)$ stays close to zero at low pressures before increasing fairly sharply.

The shape of the quadratic $f(p)$ motivates a second functional form for $f(p)$: a linear function $f(p) = f_0 + f_1p$ for $p_{min} < p < p_{max}$ which vanishes outside that range. In this case we use Equations 1 and 2 to determine f_0 and f_1 in terms of p_{min} and p_{max} : $f_0 = \frac{4\rho_3 - 6\rho_2}{4\rho_3\rho_1 - 3\rho_2^2}$ and $f_1 = \frac{3}{\rho_3} - \frac{6\rho_2\rho_3 - 9\rho_2^2}{4\rho_3^2\rho_1 - 3\rho_3\rho_2^2}$, where $\rho_n = p_{max}^n - p_{min}^n$. As before, we perform a simultaneous fit to data from various pressures, with the free parameters now being p_{min} , p_{max} , A_1 , and A_2 . The solid curves in Figure 2 are the best fits resulting from this model. The parameters p_{min} and p_{max} are 0.4 and 1.4, respectively.

We performed the same fitting procedure on data from a second sample. Although the sample is smaller and the data quality less good, we find roughly the same shape for $T_c(P)$. For both samples, and for both $f(p)$ forms, a quadratic $T_c(P)$ gives a reasonable fit, while a linear $T_c(P)$ does not.

The solid curve in Figure 3 shows $T_c(P)$ from the calculation described above, with the piecewise linear $f(p)$. Since the model produces a midpoint $T_c(P)$, we shift the solid curve upwards by 56 mK, half the transition width at zero pressure, to translate the calculated values into onset temperatures. Although the calculated $T_c(P)$ resembles the measured values, its maximum is shifted down to 1 kbar and it has more sensitivity to pressure. A variation of pressure within the sample, if it indeed occurs, can mask the pressure-dependence of the transition temperature, particularly when that dependence is not monotonic. We note that the solid curve should not be expected to agree with the measured T_c points. The measured T_c depends on nominal applied pressure, whereas the solid curve describes the expected T_c as a function of an ideal applied pressure which is uniform throughout the sample.

The pressure variation obtained from this model is much larger than anything reasonable on a macroscopic scale. A non-constant sample cross-section or an angle of the pressure spacers could cause inhomogeneity of a few percent, but the range from $0.4p_{max}$ to $1.4p_{max}$ is far too extreme. If the transition width truly signifies pressure variation, it must indicate a broad distribution of pressure within the sample from an intrinsic mechanism.

Interestingly, experiments on CeCoIn₅ under hydrostatic pressure [28] find a decrease in transition width from 80 mK at ambient pressure to 20 mK at 10 kbar. The decrease is interpreted as a consequence of tuning away from a quantum critical point near ambient pressure. We find larger changes in width at lower applied pressure, from 112 mK at ambient pressure to 270 mK at 3.97 kbar. Since uniaxial c -axis pressure may be tuning away from the quantum critical point in the opposite di-

rection from hydrostatic pressure, it seems possible that the broadening we observe is a related tuning effect.

IV. DISCUSSION

Even without the pressure measurements and analysis described above, the initial slope of the T_c curve suggests proximity to a maximum. Fits to our data suggest $\frac{dT_c}{dP}|_{P=0} = 17$ mK/kbar. The value derived from thermal expansion measurements [27] is even lower, 7.5 mK/kbar. This pressure dependence is substantially less than that of CeIrIn₅, where direct c -axis pressure measurements give $\frac{dT_c}{dP}|_{P=0} = -66$ mK/kbar [26] and thermal expansion suggests $\frac{dT_c}{dP}|_{P=0} = -89$ mK/kbar [27]. The pressure effect is also smaller than for a -axis pressure in CeCoIn₅, where thermal expansion suggests that T_c increases 29 mK/kbar [27]. One natural explanation is that CeCoIn₅ at ambient pressure is near an extremum of $\frac{dT_c}{dP}$, particularly for c -axis pressure.

Non-monotonic behavior is less common with uniaxial pressure than with its hydrostatic counterpart. Partly this is because the maximum pressure is generally much smaller in the uniaxial case, due to sample breakage or to the limits of the pressure apparatus. In addition, a given hydrostatic pressure may affect an isotropic sample in a similar way as three times as much uniaxial pressure, a consequence of applying the pressure simultaneously along all three perpendicular axes. Together these considerations mean that a typical uniaxial pressure measurement tunes a sample over a narrow regime compared to standard hydrostatic techniques.

Hydrostatic pressure measurements on CeCoIn₅ [28] find a maximum T_c near 13 kbar. Without anisotropic effects, one might expect an equivalent uniaxial pressure to be 39 kbar, since hydrostatic pressure can be viewed as uniaxial pressure applied along all three axes simultaneously. In fact, we find the maximum T_c at a drastically lower pressure near 2 kbar.

The maximum in T_c requires competing factors tending to raise or lower T_c with applied pressure. The former is the hybridization of neighboring atomic orbitals, which increases as pressure reduces the atomic spacing. Using a tight binding approximation [29–31], we estimate the fractional change in the hybridization between the Ce f -electrons and the In p -electrons as 0.0665% per kbar of c -axis pressure. An analogous calculation for CeIrIn₅ gives 0.0653% change per kbar. The similarity of these values implies that the main difference between the materials lies elsewhere.

The other key factor is sample anisotropy, which decreases with c -axis pressure. This is consistent with our maximum T_c occurring at a much lower pressure than in hydrostatic pressure measurements, since hydrostatic pressure has a more uniform effect on the sample. Calculations also predict that lower anisotropy should decrease superconducting transition temperatures [18].

The calculations track T_c/T_{sf} , where T_{sf} is the spin-

fluctuation temperature that appears to set the energy scale in magnetically mediated superconductors. In principle T_{sf} is related to the normal-phase susceptibility just above T_c . However, that susceptibility is quite small and changes only a few percent per kbar. All told the changes in χ_n are about five orders of magnitude smaller than the size of the superconducting transition. Our signal has comparable shifts from other factors, possibly including small changes in sample shape and position with applied pressure. The lack of a measurement of T_{sf} limits the comparison possible with [18]. As a rough illustration of the impact of T_{sf} , we refer to data under hydrostatic pressure [28]. There T_{sf} , which is assumed proportional to the temperature T_M of the resistance maximum, increases about 6% per kbar. We ignore anisotropy in the spin fluctuations and divide by three to adjust between hydrostatic and uniaxial pressure. We then plot T_c/T_{sf} as a function of applied c -axis pressure, shown in the inset to Figure 3. The pressure dependence of T_{sf} dominates, changing the low-pressure maximum to a near-linear monotonic decrease. Although the actual dependence of T_{sf} on c -axis pressure may differ from this estimate, for any increase of roughly the same size T_{sf} mainly determine the behavior of T_c/T_{sf} .

That T_{sf} increases with c -axis pressure is consistent with recent experiments on $\text{CeIn}_3/\text{LaIn}_3$ heterostructures [32]. As the thickness of the CeIn_3 layers decreases, the effective mass increases, an effect attributed to the changing dimensionality. Our c -axis pressure tends to increase dimensionality, which corresponds to a decreasing effective mass and increasing T_{sf} .

V. CONCLUSION

We present ac-susceptibility measurements on a single crystal sample of CeCoIn_5 under direct uniaxial pressure up to 3.97 kbar, along the c -axis. We find a weak, non-linear dependence of T_c on pressure. After an initial increase to a maximum near 2 kbar, T_c then decreases. The decrease agrees qualitatively with the behavior expected from decreasing the anisotropy parameter c/a . We also find an increase in transition width as pressure increases which is much larger than would be expected from nonuniformity in pressure and may be connected to the nearby quantum critical point.

-
- [1] J.G. Bednorz and K.A. Müller, "Possible high T_c superconductivity in the Ba-La-Cu-O system," *Z. Phys. B: Condens. Matter* **64**, 189 (1986).
 - [2] F. Steglich, J. Aarts, C.D. Bredl, W. Lieke, D. Meschede, W. Franz, and H. Schäfer, "Superconductivity in the presence of strong Pauli paramagnetism," *Phys. Rev. Lett.* **43**, 1892 (1979).
 - [3] D. Jérôme, A. Mazaud, M. Ribault, and K. Bechgaard, "Superconductivity in a synthetic organic conductor $(\text{TMTSF})_2\text{PF}_6$," *J. Physique Lett.* **41**, 95 (1980).
 - [4] Y. Kamihara, H. Hiramatsu, M. Hirano, R. Kawamura, H. Yanagi, T. Kamiya, and H. Hosono, "Iron-based layered superconductor: LaOFeP ," *J. Am. Chem. Soc.* **128**, 10012 (2006).
 - [5] C.M. Varma, P.B. Littlewood, S. Schmitt-Rink, E. Abrahams, and A.E. Ruckenstein, "Phenomenology of the normal state of Cu-O high-temperature superconductors," *Phys. Rev. Lett.* **63**, 1996 (1989); **64**, 497 (1990).
 - [6] J. Moser, M. Gabay, P. Auban-Senzier, D. Jérôme, K. Bechgaard, and J.M. Fabre, "Transverse transport in $(\text{TM})_2\text{X}$ organic conductors: possible evidence for a Luttinger liquid," *Eur. Phys. J. B* **1**, 39 (1998).
 - [7] G.R. Stewart, "Non-Fermi-liquid behavior in d - and f -electron metals," *Rev. Mod. Phys.* **73**, 797 (2001); **78**, 743 (2006); <http://rmp.aps.org>.
 - [8] W. Wu, A. McCollam, I. Swainson, P.M.C. Rourke, D.G. Rancourt, and S.R. Julian, "A novel non-Fermi-liquid state in the iron-pnictide FeCrAs ," *Europhys. Lett.* **85**, 17009 (2009); arXiv:0811.3439.
 - [9] N.D. Mathur, F.M. Grosche, S.R. Julian, I.R. Walker, D.M. Freye, R.K.W. Haselwimmer, and G.G. Lonzarich, "Magnetically mediated superconductivity in heavy fermion compounds," *Nature* **394**, 39 (1998).
 - [10] H. Kotegawa, H. Sugawara, and H. Tou, "Abrupt emergence of pressure-induced superconductivity of 34 K in SrFe_2As_2 : a resistivity study under pressure," *J. Phys. Soc. Jpn.* **78**, 013709 (2009); arXiv:0810.4856.
 - [11] L. Taillefer, "Scattering and pairing in cuprate superconductors," *Annual Rev. Cond. Matt. Phys.* **1**, 51 (2010); arXiv:1003.2972.
 - [12] C.C. Tsuei and J.R. Kirtley, "Pairing symmetry in cuprate superconductors," *Rev. Mod. Phys.* **72**, 969 (2000).
 - [13] H. Tou, Y. Kitaoka, K. Asayama, C. Geibel, C. Schank, and F. Steglich, " d -wave superconductivity in antiferromagnetic heavy-fermion compound UPd_2Al_3 – evidence from ^{27}Al NMR/NQR studies," *J. Phys. Soc. Jpn.* **64**, 725 (1995).
 - [14] O. Stockert, J. Arndt, A. Schneidewind, H. Schneider, H.S. Jeevan, C. Geibel, F. Steglich, and M. Loewenhaupt, "Magnetism and superconductivity in the heavy-fermion compound CeCu_2Si_2 studied by neutron scattering," *Physica B* **403**, 973 (2008).
 - [15] Y. Kasahara, T. Iwasawa, Y. Shimizu, H. Shishido, T. Shibauchi, I. Vekhter, and Y. Matsuda, "Thermal conductivity evidence for a $d_{x^2-y^2}$ pairing symmetry in the heavy-fermion CeIrIn_5 superconductor," *Phys. Rev. Lett.* **100**, 207003 (2008); arXiv:0712.2604.
 - [16] K. Ichimura, K. Nomura, and A. Kawamoto, "Scanning tunneling spectroscopy on organic superconductors," *Jpn. J. Appl. Phys.* **45**, 2264 (2006).
 - [17] P. Monthoux and G.G. Lonzarich, "Magnetically mediated superconductivity in quasi-two and three dimensions," *Phys. Rev. B* **63**, 54529 (2001).
 - [18] P. Monthoux and G.G. Lonzarich, "Magnetically mediated superconductivity: Crossover from cubic to

- tetragonal lattice,” *Phys. Rev. B* **66**, 224504 (2002); cond-mat/0207556.
- [19] C. Petrovic, P.G. Pagliuso, M.F. Hundley, R. Movshovich, J.L. Sarrao, J.D. Thompson, Z. Fisk, and P. Monthoux, “Heavy-fermion superconductivity in CeCoIn₅ at 2.3 K,” *J. Phys.: Condens. Matter* **13**, L337 (2001); cond-mat/0103168.
- [20] H. Hegger, C. Petrovic, E.G. Moshopoulou, M.F. Hundley, J.L. Sarrao, Z. Fisk, and J.D. Thompson, “Pressure-induced superconductivity in quasi-2D CeRhIn₅,” *Phys. Rev. Lett.* **84**, 4986 (2000).
- [21] C. Petrovic, R. Movshovich, M. Jaime, P.G. Pagliuso, M.F. Hundley, J.L. Sarrao, Z. Fisk, and J.D. Thompson, “A new heavy-fermion superconductor CeIrIn₅: a relative of the cuprates,” *Europhys. Lett.* **53**, 354 (2001); cond-mat/0012261.
- [22] J.L. Sarrao, L.A. Morales, J.D. Thompson, B.L. Scott, G.R. Stewart, F. Wastin, J. Rebizant, P. Boulet, E. Colineau, and G.H. Lander, “Plutonium-based superconductivity with a transition temperature above 18 K,” *Nature* **420**, 297 (2002).
- [23] F. Wastin, P. Boulet, J. Rebizant, E. Colineau, and G.H. Lander, “Advances in the preparation and characterization of transuranium systems,” *J. Phys.: Condens. Matter* **15**, S2279 (2003).
- [24] P.G. Pagliuso, R. Movshovich, A.D. Bianchi, M. Nicklas, N.O. Moreno, J.D. Thompson, M.F. Hundley, J.L. Sarrao, and Z. Fisk, “Multiple phase transitions in Ce(Rh,Ir,Co)In₅,” *Physica B*, **312-313**, 129 (2002); cond-mat/0107266.
- [25] J.D. Thompson, J.L. Sarrao, and F. Wastin, “Superconductivity in the isostructural heavy-fermion compounds CeMIn₅ and PuMGa₅,” *Chin. J. Phys.*, **43**, 499 (2005).
- [26] O.M. Dix, A.G. Swartz, R.J. Zieve, J. Cooley, T.R. Sayles, and M.B. Maple, “Anisotropic dependence of superconductivity on uniaxial pressure in CeIrIn₅,” *Phys. Rev. Lett.* **102**, 197001 (2009); arXiv:0908.4366.
- [27] N. Oeschler, P. Gegenwart, M. Lang, R. Movshovich, J.L. Sarrao, J.D. Thompson, and F. Steglich, “Uniaxial pressure effects on CeIrIn₅ and CeCoIn₅ studied by low-temperature thermal expansion,” *Phys. Rev. Lett.* **91**, 76402 (2003).
- [28] M. Nicklas, R. Borth, E. Lengyel, P.G. Pagliuso, J.L. Sarrao, V.A. Sidorov, G. Sparn, F. Steglich, and J.D. Thompson, “Response of the heavy-fermion superconductor CeCoIn₅ to pressure: roles of dimensionality and proximity to a quantum-critical point,” *J. Phys.: Condens. Matter* **13**, L905 (2001); cond-mat/0108319.
- [29] W.A. Harrison, *Elementary Electronic Structure*, (World Scientific Publishing Co., Singapore, 1999)
- [30] J.M. Wills and W.A. Harrison, “Interionic interactions in transition metals,” *Phys. Rev. B* **28**, 4363 (1983).
- [31] R.S. Kumar, A.L. Cornelius, and J.L. Sarrao, “Compressibility of CeMIn₅ and Ce₂MIn₈ (M=Rh, Ir, and Co) compounds,” *Phys. Rev. B* **70**, 214526 (2004); cond-mat/0405043.
- [32] H. Shishido, T. Shibauchi, K. Yasu, T. Kato, H. Kontani, T. Terashima, Y. Matsuda, “Tuning the dimensionality of the heavy fermion compound CeIn₃,” *Science* **327**, 980 (2010).